Optical Sensing with a Potentiometric Sensing Array by Prussian Blue Film Integrated Closed Bipolar Electrodes

Jansod, Sutida; Cherubini, Thomas John; Soda, Yoshiki; Bakker, Eric

How to cite

JANSOD, Sutida et al. Optical Sensing with a Potentiometric Sensing Array by Prussian Blue Film Integrated Closed Bipolar Electrodes. In: Analytical Chemistry, 2020, vol. 92, n° 13, p. 9138–9145. doi: 10.1021/acs.analchem.0c01421

This publication URL: https://archive-ouverte.unige.ch/unige:141063
Publication DOI: 10.1021/acs.analchem.0c01421

analytical chemistry

pubs.acs.org/ac Article

Optical Sensing with a Potentiometric Sensing Array by Prussian Blue Film Integrated Closed Bipolar Electrodes

Sutida Jansod, Thomas Cherubini, Yoshiki Soda, and Eric Bakker*

Cite This: *Anal. Chem.* 2020, 92, 9138−9145 Read Online

ACCESS | Metrics & More | Article Recommendations | Supporting Information

ABSTRACT: The simultaneous optical readout of a potentiometric sensor array of ion-selective electrodes (ISEs) based on PVC membranes is described here for the first time. The optical array consists of electrochromic Prussian Blue (PB) films in multiple closed ion-selective bipolar electrodes (BPEs), which gives a physical separation between the optical detection and sample compartments. The potential-dependent turnover of PB generates Prussian White (PW). A near-Nernstian response of the PB film is confirmed by colorimetric absorbance experiments as a function of applied potential. In the combined bipolar electrode cell, the overall potential is kept constant with a single potentiostat over the entire array where each PB spot indicates the potential change of an individual connected potentiometric probe. For cation-selective electrodes, the absorbance or blue intensity of the connected PB film is enhanced with increasing target cation activity. The colorimetric absorbance changes are simultaneously followed by a digital camera and analyzed by Mathematica software. A multiple cation-BPE array allows one to achieve simultaneous quantitative analysis of potassium, sodium, and calcium ions, demonstrated here in highly colored fruit juices. Mass transport at the PB thin film is shown not to be rate-limiting. The measuring ranges can be tuned in a wide range by potential control. The PB film exhibits greatly improved reproducibility and stability as compared to previous work with a ferroin redox probe confined in a thin solution layer.

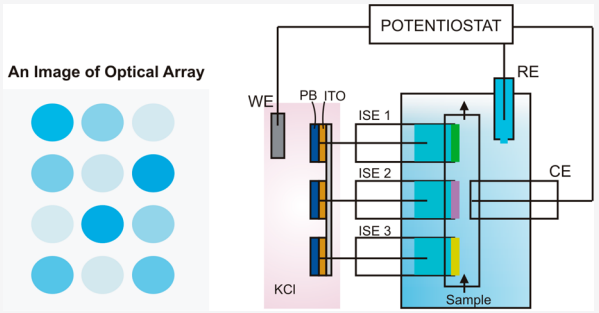

Sensor arrays are used to simultaneously identify multiple target ions in complex mixtures.[1−3] They are particularly useful in clinical and environmental analysis, either for imaging or mapping one or more chemical species[4] or for assessing multiple analytes.[5,6]

Potentiometric sensors based on liquid or polymer membrane material such as ion-selective electrodes (ISEs) combine advantages of adequate selectivity, sensitivity, reproducibility, and response time.[7−11] The selective membrane of ISEs is the key component that allows for the recognition of the target ion. Potentiometric sensor arrays have been used for multivariate analysis[12,13] and are becoming important for the realization of in situ sensing tools.[14−16] Moreover, ISE arrays may be miniaturized for flow applications[17,18] that may give a high sample throughput and allow for small sample volumes, for example, in bioanalysis. In environmental analysis, potentiometric sensor arrays have been used in the quantitative analysis of pH, potassium, sodium, calcium, nitrate, carbonate, and ammonium.[15,19,20]

Array sensing platforms based on optical sensors have become important for the determination of multiple analytes, to assess near-complete chemical information for a given sample, and to achieve real-time chemical imaging.[21−24] However, traditional optical sensors may be negatively affected by turbid or colored samples, as the working ranges are comparatively narrow and the detection of ions requires extra-thermodynamic assumptions that are not always well understood or accepted. Such drawbacks may be overcome by coupling their output to a potentiometric probe using closed bipolar electrodes (BPEs) where the sample solution is physically separated from the site of the optical signal change.[25−27]

In this manner, potentiometric signals have been transduced to a series of different optical readouts, such as electrochemiluminescence (ECL).[28] The potential change at the ISE acted as the reference electrode in the sample compartment. The working electrode activated the ECL output in the detection solution when a constant potential was applied across the cell. In other work, the light output of multicolor light-emitting diodes (LEDs)[29] was coupled to the potentiometric response of ISEs by chronoamperometry control. A fluorescence signal was also obtained from a solid-contact ISE containing polypyrrole as ion-to-electron transducing material and connected to a zinc element in the same compartment.[30]

Received: April 2, 2020
Accepted: June 2, 2020
Published: June 2, 2020

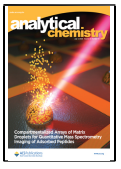

https://dx.doi.org/10.1021/acs.analchem.0c01421
Anal. Chem. 2020, 92, 9138−9145

An increasing ion activity triggered the reduction of the polypyrrole and resulted in the oxidation of zinc in another pole. This increased the emission intensity where the charge served as an analytical signal. Unfortunately, the emission obtained by ECL, LEDs, and florescence have some drawbacks such as (i) the detection must be controlled in the dark, (ii) specific instruments, reagents, and materials tend to be costly, and (iii) they are not yet applicable for optical sensor arrays.

Alternatively, the water-soluble redox indicator ferroin was proposed to translate the potential change at ISEs in closed-BPEs.[31,32] This general approach is promising for the fabrication of a large sensor array. The optical signal was captured by just a digital camera in ambient light, whereas the ECL, LEDs, and florescence were limited to the dark. However, the ferroin indicator requires a dedicated thin layer cell to reduce evaporation losses and allow for an exhaustive turnover in a reasonable amount of time. To overcome these drawbacks, an electrochromic thin film deposited on a conductive electrode surface may be instead used as the optical indicator. Examples include tungsten oxide (WO_3),[33] polymeric viologen,[34,35] and conjugated conducting polymers such as PEDOT[36] and Prussian Blue (PB).[37−40] These electrochromic materials may change their optical properties by a redox process and/or a suitable electrochemical potential.

PB (anodic form) is known as an important functional transition metal hexacyanoferrate with stable electrochemical redox behavior and excellent electrochromic properties, which makes it a prominent candidate as an electrochromic indicator.[41] The intense blue color of PB, iron(III) hexacyanoferrate(II) chromophore, increases from intervalence charge transfer between the mixed-valence iron oxidation by the redox process.[42] The electrochemical reduction of PB produces Prussian White (PW) or iron(II) hexacyanoferrate-(II), which becomes transparent as a thin film. The electrochemical deposition of PB films in aqueous solution onto conducting substrates was first described by Neff.[43] The films were prepared in a mixed solution of $FeCl_3$ and $K_3Fe(CN)_6$ in an excess of KCl. A high concentration of KCl accelerates the PB conversion process.[44]

In 2001, Lin's group used PB film deposited onto tin oxide electrode to directly measure potassium ion using cyclic voltammetry. This PB film served as a mediator for potassium ion transfer. The voltammograms shifted with increasing potassium concentration, which resulted in a sub-Nernstian response slope.[45] In 2009, Toh's group used a PB nanotube sensor for potassium detection by using cyclic voltammetry. The peaks shifted with a near-Nernstian slope to anodic potentials with increasing potassium concentration.[46] More recently, Rieger's group used PB nanoparticles on a screen-printed carbon electrode covered by a sodium ion-selective membrane for sodium detection. However, this approach exhibited sub-Nernstian response with a limited working range.[47] No reports have used PB thin film as a redox indicator by coupling to potentiometric sensing probes in a bipolar electrode arrangement.

We describe here a closed multiple ion-selective BPE sensor array for the simultaneous detection of multiple analytes with working ranges that can be tuned by the applied potential. This approach demonstrates the translation of potentiometric responses based on ISEs into optical PB thin films. The multiple ion-selective BPEs array allows one to access all quantitative information from each individual BPE. The slopes obtained by the ISEs are near-Nernstian. The conversion of PB/PW is correlated in a Nernstian manner to the BPE response. In this way, colorimetric absorbance can be used to directly detect the concentration (activity) of the target ions.

PRINCIPLE OF OPERATION

As demonstrated in Scheme 1, each ISE is individually coupled to one PB film in a bipolar arrangement. The cell potential is kept constant by a potentiostat. As the cation activity in the sample increases, it generates a more positive potentiometric signal at the ISE. This potential change must be compensated by an opposite change at the PB film, resulting in the partial oxidation of PW to PB to satisfy the Nernst equation. This results in an absorbance change of the PB film, which serves as the analytical signal. Any number of parallel bipolar ISE−PB pairs may be inserted into the cell to give a convenient optical readout of the sensing array.

The response to sample activity change is transient and ceases upon reaching each new electrochemical equilibrium state. During the transient and for an increasing sample activity change, the cation of interest is extracted and transported across the ion-selective membrane (ISM in Scheme 1), and thereby triggers the partial reduction of the Ag/AgCl element, which releases chloride into the inner solution to maintain

Scheme 1. Construction of Ion-Selective BPE(s), Where the Optical Detection Compartment Is Physically Separated from the Sample Compartment[a]

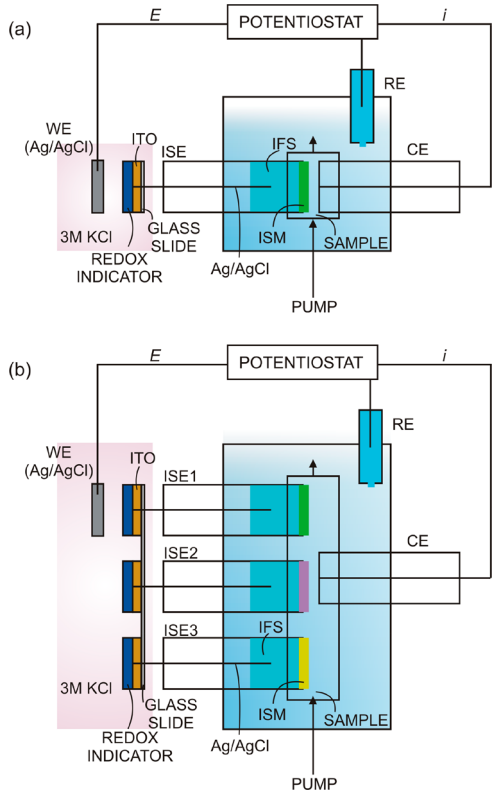

[a](a) Classical ion-selective BPE contains a single ISE, which couples to a PB film. (b) Multiple ion-selective BPEs sensor array contains multiple ISEs, which couple to multiple PB films. Each BPE is disconnected from each other. The potential is applied across a working electrode (WE) in the detention compartment and a counter electrode (CE), and a double junction reference electrode (RE) in the sample compartment.

https://dx.doi.org/10.1021/acs.analchem.0c01421
Anal. Chem. 2020, 92, 9138−9145

charge balance. The electrons required for this reduction process originate from oxidation at the other end of the bipolar electrode, where PW partially converts to PB. To compensate, this releases potassium ions into the contacting solution. The Ag/AgCl elements placed in solution complete the circuit.

Each closed bipolar electrode in the array is an ISE in contact with the sample and connected to a transparent electrode coated with an electrochromic Prussian Blue film in a separate detection cell. Scheme 1a shows one such BPE where a single potentiometric probe is coupled to the PB thin film. Scheme 1b then illustrates how a multiple ion-selective BPEs sensor array can be likewise coupled to an array of PB thin films.

The electrochemical cell used for the detection of analyte ion i of valency z is of the type:

Ag|AgCl|3 M KCl|PB film|ITO|Ag|AgCl|iCl$_z$(IFS)|ISE membrane|iCl$_z$ (sample)||1 M LiOAc|3 M KCl (aq)|AgCl|Ag

where PB functions as the colorimetric redox probe; ITO is a indium tin oxide-based transparent electrode; IFS is the inner filling solution of the membrane electrode; ISE membrane is the ion-selective membrane; and $i\mathrm{Cl}_z$ is the chloride salt of the analyte cation. In the absence of interference, the potential across the ion-selective membrane, E_M, is described as established by eq 1:

$$E_M = \frac{s}{z_i} \log \frac{a_i^{\text{sample}}}{a_i^{\text{ifs}}} \tag{1}$$

where s is the Nernstian slope for a monovalent cation, ideally 59.2 mV for 25 °C, and a_i is the activity of i in the sample or inner filling solution (IFS) on either side of the membrane, as indicated.

The detection compartment contains a PB film used as the optical redox indicator, which changes its color from colorless (PW, reduced form) to blue (PB, oxidized form). The standard reduction potential of PB has been reported as 0.238 V vs Ag/AgCl at 25 °C.[48] The corresponding half-reaction for PB may be given as[49]

$$\underset{(\text{PB})}{\mathrm{KFe^{III}[Fe^{II}(CN)_6]_{(film)}}} + \mathrm{K^+_{(aq)}} + \mathrm{e^-} \rightleftharpoons \underset{(\text{PW})}{\mathrm{K_2Fe^{II}[Fe^{II}(CN)_6]_{(film)}}} \tag{2}$$

The reduction of PB is accompanied by the incorporation of potassium ion, which makes this system an ion to electron transducing material.

While PB is a polymeric material, we may attempt to describe the potential of a mixed PW/PB film in contact with a solution of constant potassium concentration in a Nernstian manner,[45] as shown in eq 3:

$$E_{\text{detection}} = E^0_{\text{PW/PB}} - s \log \frac{c_{\text{PW}}}{c_{\text{PB}}} + s \log a_K^{\text{aq}} \tag{3}$$

where C_{PW} and C_{PB} are the apparent film concentrations of PW and PB, respectively. If so, these concentrations may be expressed as a function of colorimetric absorbance based on Beer's law as shown in eq 4. A_{max} and A_{PB} are the absorbances at the maximum and at a given PB equilibrium state, respectively; see the Supporting Information for the derivation of the equations.

$$E_{\text{detection}} = E^0_{\text{PW/PB}} - s \log \frac{A_{\text{max}} - A_{\text{PB}}}{A_{\text{PB}}} + s \log a_K^{\text{aq}} \tag{4}$$

In a closed-bipolar platform, the redox indicating PB film is connected in series to the ISE. The overall potential of the cell (E_{cell}) is described by eq 5 as

$$E_{\text{cell}} = s \log \frac{A_{\text{max}} - A_{\text{PB}}}{A_{\text{PB}}} + \frac{s}{z_i} \log a_i^{\text{sample}} + E_{\text{const}} \tag{5}$$

Here, E_{cell} is imposed by the potentiostat, and the absorbance ratio of PW/PB is a function of the sample activity a_i as shown. Consequently, the potential imposed as E_{cell} can be used to adapt the optical signal to the desired measuring range (see the Supporting Information). The PB absorbance is then expressed as

$$A_{\text{PB}} = A_{\text{max}} \left(\frac{\psi}{a_i^{1/z_i}} + 1 \right)^{-1} \tag{6}$$

with

$$\psi = 10^{(E_{\text{cell}} - E_{\text{const}})/s} \tag{7}$$

For a constant applied potential, E_{cell}, and a cation-selective electrode, an increasing cation activity in the sample results in a higher PB absorbance.

The absorbance may also be obtained by a digital camera, where the recorded images are analyzed in analogy to spectrophotometry.[50] Here, the PB absorbance is calculated by the acquired red channel image; see eq 8 in the Experimental Section.

EXPERIMENTAL SECTION

Materials, Reagents, and Instrumentation. Potassium chloride (KCl), sodium chloride (NaCl), calcium chloride ($CaCl_2$), magnesium chloride ($MgCl_2$), hydrochloric acid (HCl), sodium hydroxide (NaOH, 1.0 N), potassium ionophore I, sodium ionophore X, calcium ionophore IV, poly(vinyl-chloride) (PVC, high molecular weight), dodecyl 2-nitrophenyl ether (DD-NPE), sodium tetrakis-[3,5-bis-(trifluoromethyl)phenyl]borate (NaTFPB), tetradodecylammonium tetrakis(4-chlorophenyl)borate salt (ETH 500), tetrahydrofuran (THF), indium tin oxide (ITO glass slide 25 mm × 25 mm × 1.1 mm, surface resistivity 1.28−1.92 Ω cm^{-2}), iron(III) chloride hexahydrate ($FeCl_3 \cdot 6H_2O$), potassium hexacyanoferrate(III) ($K_3[Fe(CN)_6]$), and Whatmann qualitative filter paper grade 2 were purchased from Sigma-Aldrich. An insulating transparent Scotch 3 M tape (50 μm thickness) and a metallic hole punch tool (0.8 mm diameter) were used. An Ag electrode tip with a diameter of 3.00 ± 0.05 mm (6.1204.330) was sourced from Metrohm (Switzerland). An IPC ISMATEC peristaltic pump (model ISM935C, Clattbrug, Switzerland), TYGON tubing (inner diameter 1.42 mm, wall 0.86 mm), and PTFE tubing (L × OD × ID = 300 mm × 1/16 × 100 μm, Supelco) were used in the flow system. The electrochemical measurements of cyclic voltammetry and chronoamperometry were performed in a faraday cage with a potentiostat/galvanostat PGSTAT 204 (Metrohm Autolab, Utrecht, The Netherlands) that was controlled by Nova 2.1.2 software. A tethered digital camera (Canon EOS 5D Mark II) equipped with a MP-E 60 mm macro lens and matching ring flash was used to capture the images from the detection cell. Real samples were purchased at a local market.

https://dx.doi.org/10.1021/acs.analchem.0c01421
Anal. Chem. 2020, 92, 9138−9145

All aqueous solutions were prepared in Milli-Q water. The background electrolyte was 10 mM $MgCl_2$. A studio shooting tent box was purchased from PULUZ Technology Limited (Shenzhen, China).

Fabrication of Patterned ITO Array. A conductive ITO film-coated glass electrode (25 × 25 × 1.1 mm) was etched into three films or channels, as an example. To etch the master ITO film, the glass electrode was entirely covered by the tape. A tiny gap was exposed by a cutter. This exposed area was vanished by immersion in concentrated HCl for 10−20 min. The entire tape was removed. The patterned ITO array was rinsed many times by Milli-Q water until there was no acid residue left on the electrode. It was then dried at room temperature. The surface resistivity of the etched tiny gap was measured by a digital ohmmeter. If these channels were disconnected or isolated from each other, the resistance value of this exposed area should not be found. The patterned ITO array contained three channels in the same glass; see the photograph in the Supporting Information.

PB Film Deposition. Three circular openings of 0.8 mm diameter were punched in a 50 μm thick adhesive insulating tape to form recesses. This tape was placed on the patterned ITO array. In the electrochemical cell, the ITO electrode acted as the working electrode, the platinum rod was the counter electrode, and the Ag/AgCl wire was the reference electrode. The ITO electrode was immersed in the mixed solution of 20 mM $K_3Fe(CN)_6$, 20 mM $FeCl_3{\cdot}6H_2O$, and 10 mM HCl. The PB film was deposited for 20 s by passing a cathodic current density of 2.0 A m^{-2} through the ITO electrode. Each channel was individually deposited; see the photograph of three PB electrodes in the Supporting Information. The PB sensor array was washed by 10 mM HCl before use.

Stabilization of the PB Film. A PB electrode acted as a working electrode, and the Ag/AgCl wire was the counter/reference electrodes. The PB was first stabilized by using cyclic voltammetry. All electrodes were immersed in 3 M KCl (pH 2, adjusted the pH by using HCl). The potential was reversibly applied between 0.4 and 0.2 V vs Ag/AgCl for 15 cycles with a scan rate of 10 mV s^{-1} before use in the BPE. The PB film was characterized by applying cathodic and anodic linear potential scans at a scan rate of 0.5 mV s^{-1}. The PB absorbance and the integrated charge were observed as a function of applied potential. The images were consecutively captured by the camera every 10 s. All images were computed from the PB film from all residual pixels into absorbance with eq 8.

PB Film Removal. The PB film deposited on the ITO electrode was effectively removed by rinsing with 10 mM NaOH followed by an abundance of Milli-Q water. The ITO electrode was dried at room temperature before use.

Preparation of Potentiometric Sensing Electrodes. A mixture of ionophore (15 mmol kg^{-1}), ion exchanger (5 mmol kg^{-1}), ETH 500 (90 mmol kg^{-1}), PVC, and DD-NPE plasticizer (1:2 by weight; total mass 200 mg) was prepared for potentiometric sensing probe, as reported in our previous work.[32] The components were dissolved in 2 mL of THF and poured into a glass ring (22 mm i.d.) fixed on a glass slide with rubber bands. The solution was evaporated overnight at room temperature. The homogeneous master membrane was punched into disks of 8 mm diameter (200−300 μm thickness). The membranes were conditioned in 1 mM of primary ion for at least 3−4 h. The membrane was mounted in an Ostec electrode body (Oesch Sensor Technology, Sargans, Switzerland). The inner filling solution (IFS) in the ISE for the determination of potassium, sodium, and calcium was filled with 1 mM KCl, 1 mM NaCl, and 1 mM $CaCl_2$, respectively.

Sample Compartment. The potentiometric measurement of ISE-based PVC membranes was carried out against a commercial reference electrode (6.0729.100, Metrohm) with a double junction reference electrode (Ag|AgCl|KCl, 3 M|LiOAc, 1 M) in a Faraday cage using a 16-channel EMF interface (Lawson Laboratories, Inc., Malvern, PA). The K-ISE, Na-ISE, Ca-ISE, and Ag counter electrode were placed in the flow cell, separated by a narrow solution channel, to which the ion is transported to the ISEs by a peristaltic pump through the inlet and waste to bulk solution through the outlet; see the photograph of the flow cell in the Supporting Information. The reference electrode was placed in the bulk solution in the beaker. All solutions were maintained in 10 mM $MgCl_2$. Real samples were filtered by filter paper and diluted 5-fold with $MgCl_2$ solution before being introduced to the sample cell.

Detection Compartment. The PB array on the glass electrode was inserted in the detection cell, which contains 3 M KCl (pH 2). The image was captured in the white bright studio shooting tent at ISO 400, f/5.0, flash power 1/128. The camera was set in front of the tent. The optical signals were recorded with a tethered digital camera (Canon EOS 5D Mark II) equipped with a Canon MP-E 60 mm macro lens and a ring flash. Only the macro lens with the ring flash was in the tent. The camera captured all images in JPEG format, which were analyzed for absorbance. This involved importing each image, automatic cropping for the detection compartment area, and computing the absorbance from the red channel as shown in eq 8.

Experimentally, the absorbance of the PB film, which serves as an optical redox indictor, can be obtained by computing the color intensity by Mathematica software 11.1 (Wolfram Research). Consecutive images were captured by a digital camera. The colorimetric absorbance (A) for any of the three color channels, R, G, or B, was determined as described recently.[50] For the red channel:

$$A(\mathrm{R}) = -\frac{1}{\gamma}\log\frac{I(\mathrm{R})}{I_0(\mathrm{R})} \tag{8}$$

where $I(\mathrm{R})$ and $I_0(\mathrm{R})$ are the recorded red channel intensities of the PB film and the background, respectively. γ is the gamma correction ($\gamma = 1/2$) applied in the camera to make the image output more realistic to the human eye. The observed absorbance (A) from the image was obtained after removing gamma correction as shown in eq 8.

Construction of Ion-Selective BPE. The optical PB electrode was individually coupled to the ISE in the sample cell with the closed BPE configuration, as shown in Scheme 1. The potential was applied between the Ag/AgCl wire (WE) in the detection cell and the Ag counter electrode (CE), and the double junction reference electrodes (RE) in the sample compartment; see the photograph in the Supporting Information.

RESULTS AND DISCUSSION

Characterization of PB Films. Figure S1 shows the cyclic voltammogram of the turnover of the PB thin film deposited on the ITO electrode in 3 M KCl (pH 2). The reduction potential of PB in 1 M KCl was found at 0.216 ± 0.0006 V vs Ag/AgCl. For the conditions used here, the charge of the PB film was found as 7.48 ± 0.08 and 7.53 ± 0.15 μC for the

https://dx.doi.org/10.1021/acs.analchem.0c01421
Anal. Chem. 2020, 92, 9138−9145

anodic and cathodic peaks, respectively. Figure S2 (left) gives the typical Gaussian shape of the corresponding voltammetric waves at different scan rates upon electrochemical oxidation/reduction of the PB redox indicator. A thin layer behavior of the PB membrane was confirmed, as evidenced by the linear dependence of peak height current with scan rate. This indicates that mass transport is not rate-limiting under these conditions; see Figure S2 (right). Figure S3a shows the corresponding change of integrated charge with different applied potentials, when anodic and cathodic potentials are applied by cyclic voltammetry to the detection cell only. This potential scan allows one to observe the PB absorbance change, as shown in Figure 1 (left). The absorbance does

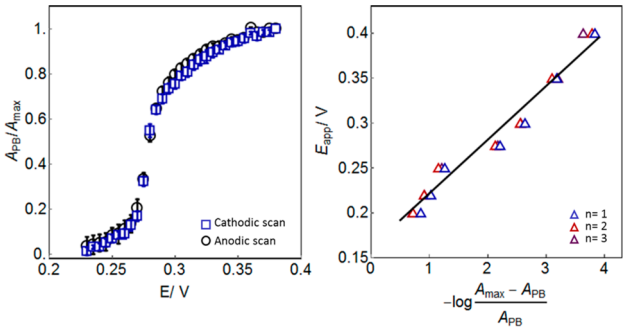

Figure 1. (Left) Absorbance with constant applied potential. The scan rate is 0.5 mV s^{-1}. (Right) Observed linear relationship between the discrete applied potentials and the logarithmic concentration ratio of PB/PW from colorimetric absorbance, which demonstrates near-Nernstian behavior in reasonable agreement with eq 4.

increase with increasing integrated charge (Figure S3b), although a deviation from linear behavior is observed. The deviation was minimized by applying constant potential increments instead of a linear scan. Figure 1 (right) demonstrates a near-Nernstian response (slope of 60.7 mV) of the optical redox indicator, in reasonable agreement with eq 4.

Figure 2 demonstrates the reproducibility and stability of the PB film when subjecting it to alternating potentials of 0.3 and 0.2 V, which results in corresponding red channel colorimetric absorbance values of 0.151 ± 0.3% (translating into 2% uncertainty in activity determination by eq 6) and 0.0183 ± 0.1% (corresponding to a 5.9% uncertainty in activity). The images were captured every 6 s. The response time was found

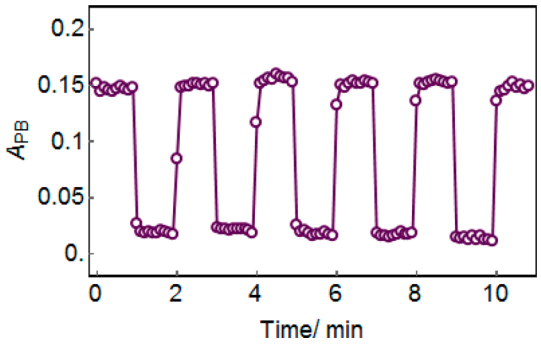

Figure 2. Corresponding PB absorbance changes in the detection compartment. The constant potentials of 0.3 and 0.2 V are imposed on the PB electrode in the detection cell only. All electrodes are immersed in 3 M KCl (pH 2).

as $t_{95\%}$ = 11 s. The absorbance change follows the potential change rapidly, in agreement with the absence of mass transport limitation noted above.

Characterization of the Potentiometric Sensor Array Flow Cell. An array of three cation-selective electrodes (ISEs) was used in the sample compartment. All were ionophore-doped sensing membranes individually selective toward their target ion. The observed logarithmic selectivity coefficients for the prepared membranes have been reported earlier.[32] The flow cell was designed to accommodate numerous ISEs so that multiple analytes can be simultaneously measured in a selective manner. Figure S4 (left) shows the potentiometric calibration curves of the K-ISE, Na-ISE, and Ca-ISE. These potentiometric probes were simultaneously characterized by open circuit potentiometry in mixed solutions containing the chloride salts of potassium, sodium, and calcium, with magnesium salt as the background electrolyte. The potentiometric probes were confirmed to exhibit near-Nernstian response slopes to the activities of potassium (58.6 ± 0.1 mV), sodium (58.0 ± 0.7 mV), and calcium (29.6 ± 0.6 mV). The corresponding potential−time traces (n = 3) are shown in Figure S4 (right).

The sample flow cell was confirmed to be free of solution carry-over by alternating the solution between 1 and 10 mM of KCl, NaCl, and $CaCl_2$; see Figure S5 (left). The peristaltic pump required about 60 s to replace each solution and to allow for the potentiometric signal to stabilize. Replicate measurements exhibited small deviations (maximum deviation was 0.6 mV, n = 3); see Figure S5 (right).

The conversion of the PB film triggered by the potential change at the corresponding potentiometric probe is accompanied by an electrical charge that passes through the cell. To evaluate its effect on the potentiometric probe, the same charge (7.5 μC) was applied to the potentiometric probe individually by imposing 0.25 μA for 30 s to the Na-ISE. The electrochemical perturbation resulted in a brief potential excursion of 17 mV before returning to the new equilibrium state within 2 min; see Figure S6. This suggests that the optical readout of the PB film accurately reflects the potential change at the ISE after stabilization, once the transient current is again near zero.

Characterization of a Closed BPE Containing a Single ISE. For an ion-selective bipolar electrode, the PB spot indicates the potential change of its individual, connected potentiometric probe. A sample activity change at the ISE results in a well-defined potential change (EMF). Here, E_{cell} is maintained to a constant value, and the potential change at the ISE is compensated by an opposite potential change of equal amplitude at the PB film-coated ITO electrode. At an appropriate applied potential value, this results in an absorbance change of the PB film until the new electrochemical equilibrium state is reached. The colorimetric absorbance was captured by a camera and analyzed with eq 8.

Figure 3a shows the normalized current responses of a Na^+-selective BPE with a 10-fold increase in sample concentration. The bell-shape current response demonstrates that the current is limited by the conversion of PW/PB. The peak shifts to a more anodic potential with increasing sodium activity (slope of 59.2 mV per 10-fold sodium activity change in sample compartment). Figure 3b demonstrates the corresponding absorbance change and confirms the potential modulation at the detection cell by the ion-selective probe. The sigmoidal calibration curves are described by eq 6. The absorbance

https://dx.doi.org/10.1021/acs.analchem.0c01421
Anal. Chem. 2020, 92, 9138−9145

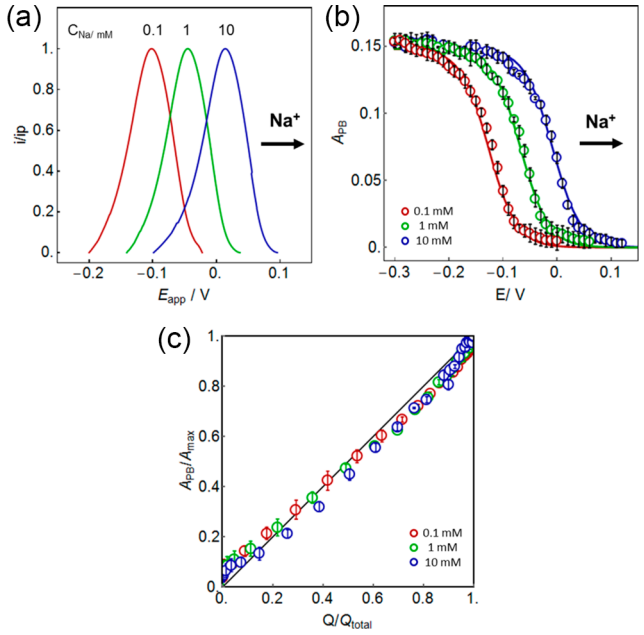

Figure 3. (a) Normalized current responses of the classical Na-BPE. The scan rate is 1 mV s^{-1}. (b) Observed absorbance in the detection compartment at each applied potential and with the increase sodium concentrations of 0.1, 1, and 10 mM NaCl in the sample compartment. The calibration curves are simulated by using eq 6. (c) A linear relationship between the PB absorbance and the PB charge in Na-BPE. Error bars are standard deviations (n = 3).

change of redox indicator PB correlates linearly with the charge passed through the cell; see Figure 3c.

The corresponding current responses for K^+-selective and Ca^{2+}-selective BPEs are shown in Figure S7 (top). The peak is found to shift by 61.6 and 32.0 mV per 10-fold potassium and calcium activity change, respectively, which agrees with the Nernstian slope. The absorbance-based calibration curves shift in the same manner to more anodic potentials with increasing ion activity in the sample, Figure S7 (bottom). This anodic shift demonstrates that the measuring range of the optical PB indicator can be electrochemically tuned.

Characterization of the Closed BPE Array. Cation-selective electrodes for K^+, Na^+, and Ca^{2+} were combined into a BPE sensor array as schematically shown in Scheme 1b.

Figure 4 shows the resulting absorbance-based calibration curves for Na-BPE in a single configuration (colored symbols) and multiple electrode array (black symbols), using applied potentials of −150, −100, and −50 mV for the three calibration curves as shown. No discrepancy for the observed absorbance values in single and multiple electrode configurations was observed, which suggests a lack of cross-talk between the three bipolar electrodes. For the best analytical results, the absorbance-based calibration curves are here fitted sigmoidals based on the Boltzmann equation.[51] The corresponding calibration curves of the K-BPE (Figure S8, left) and Ca-BPE (Figure S8, right) in both single and BPEs array configurations are shown in the Supporting Information. In all cases, the PB absorbance values correspond well with the fitted calibration curves, which suggests that a single image of the PB array can be used to assess multiple cations in the sample.

The stability and reproducibility of the BPE were characterized by alternating the applied potential values. Figure S9 shows the reversibility of the PB electrode in the bipolar arrangement by switching the applied potential between −120 and −150 mV in the Na-BPE, with the sample cell containing 0.1 mM NaCl. This resulted in an absorbance change between 0.038 ± 0.05% (1.4% uncertainty in activity) and 0.095 ± 0.1% (1% uncertainty in activity), respectively. In the BPE arrangement, the optical signal responds more slowly than for the detection cell only ($t_{95\%}$ = 65 s, compare with Figure 2). This slower equilibration is explained with the transient potential at the ion-selective electrode upon the passage of current; see above. This does not influence the final absorbance, as the analysis is performed after electrochemical equilibrium is established where the current again approaches zero.

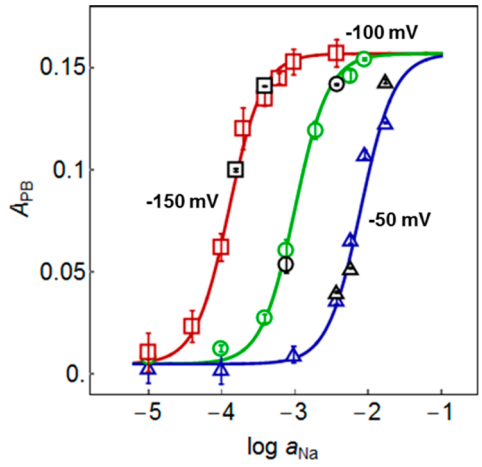

Figure 4. PB absorbance and logarithmic sodium activity of Na-BPE in classical BPE (colored symbols) and multiple BPE arrays (black symbols) at three different constant applied potentials. The sigmoidal calibration curves are fitted by using the Boltzmann equation.

Selectivity in Multiple BPEs Array. In the BPE array, the cations of interest are simultaneously determined in mixtures of KCl, NaCl, and $CaCl_2$. The selectivity coefficients of the ISEs have been reported in our previous work,[32] so here each individual BPE in the sensor array was analyzed to ensure that the optical response of each channel remains selective to its associated target ion.

Figure 5 traces the absorbance values of three different channels in the multiple cation-BPE array containing the three ISEs selective for Na^+, K^+, and Ca^{2+} with an applied potential of −100 mV. The introduction of 1 mM NaCl into the sample cell results in a higher PB absorbance only for the Na-BPE,

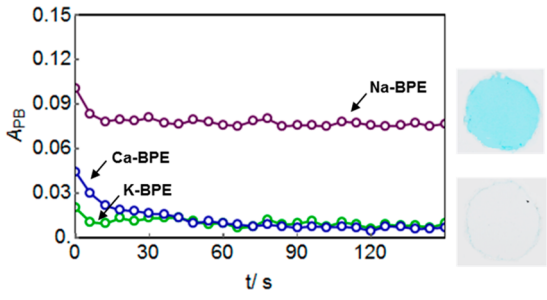

Figure 5. Absorbance values of Na-BPE (purple), K-BPE (green), and Ca-BPE (blue) are changed, when a constant potential of −100 mV is imposed in the multiple BPEs array. The sample solution contains only 1 mM NaCl.

https://dx.doi.org/10.1021/acs.analchem.0c01421
Anal. Chem. 2020, 92, 9138−9145

while it remains unchanged at the K^+ and Ca^{2+}-BPEs. Similarly, a higher PB absorbance was only observed for the K-BPE (Figure S10, left) and Ca-BPE (Figure S10, right), when the sample contained only 1 mM KCl and 1 mM $CaCl_2$, respectively. Figure S11 shows the corresponding images of the PB spots in the detection compartment. This experiment confirms that each individual BPE in the BPE array is highly selective toward its target ion.

Analysis of Real-World Samples by the Cation-BPE Array. The cation-selective BPE array was used to simultaneously determine the concentrations of potassium, sodium, and calcium ions in colored juice samples, including orange, grape, multifruit, and coconut juices. Different constant potentials were applied to the cation-selective BPE array to obtain the appropriate absorbance changes that reflect the dynamic range for the samples. When an applied potential of −100 mV was imposed to the BPE array, the PB absorbance for the Na-BPE and K-BPE was found to change, which allowed one to simultaneously measure the sodium content in grape and multifruit juices and the potassium level in coconut juice. When a constant potential of −50 mV was imposed, the K-BPE could be used to assay potassium in orange, grape, and multifruit juices and sodium in coconut juice by the Na-BPE. With a more cathodic potential of −150 mV, the PB absorbance changed for the Na-BPE in orange juice. Calcium ions for all samples were measured by applying a potential of −170 mV.

The corresponding images captured in the detection compartment are shown in Figure 6. The absorbance values

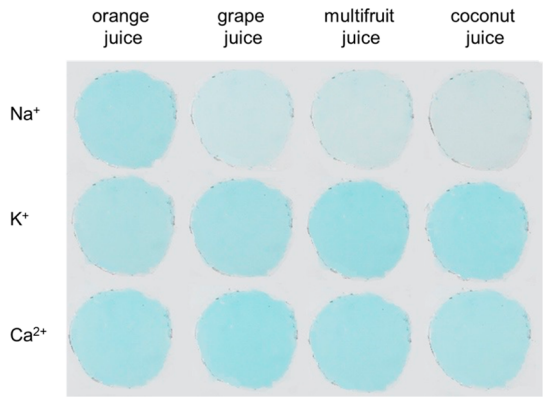

Figure 6. Images of the colorimetric sensor array acquired in the detection compartment for different samples coupled to their respective cation-selective BPEs. For this experiment, different constant potentials are imposed, and the absorbance values correlating to sodium, potassium, and calcium concentration are compared to the respective calibration curves as shown in Figure S12.

for sodium, potassium, and calcium are plotted on the sigmoidal calibration curves at the corresponding applied potential, as shown in Figure S12. The observed absorbance is converted to the predicted concentration as shown in Table 1. The results correlate well with those from direct potentiometry, used here as the reference method.

The ISE exhibits great stability and reproducibility, and it can be stored for at least 30 days.[32] The PB film also shows good reproducibility and can be used for at least 85 cycles (Figure S13). The PB deposited on the ITO electrode can be easily disposed of by rinsing with 10 mM NaOH. The ITO electrode can be reused again for a new PB film deposition.

Table 1. Determination of Sodium, Potassium, and Calcium Concentrations (mM) in Various Juices Using the Multiple Cation-Selective BPE Array (SD, n = 3)[a]

samples	Na/mM	K/mM	Ca/mM
orange juice: BPE	0.85 ± 0.09	43.0 ± 0.8	4.09 ± 0.09
potentiometry	$0.86 \pm 0.00_2$	45.7 ± 0.02	4.4 ± 0.2
grape juice: BPE	2.96 ± 0.05	29.6 ± 1.8	5.28 ± 0.08
potentiometry	2.9 ± 0.2	$29.5 \pm 0.0_1$	$5.7_4 \pm 0.2_5$
multifruit juice: BPE	2.34 ± 0.05	48.7 ± 1.4	4.3 ± 0.2
potentiometry	2.1 ± 0.3	45.5 ± 0.3	$4.3 \pm 0.0_5$
coconut juice: BPE	14.7 ± 0.4	$8.1_5 \pm 0.1$	3.43 ± 0.09
potentiometry	14.8 ± 0.6	8.03 ± 0.04	$3.40 \pm 0.00_4$

[a]Potentiometry is used as a reference method.

CONCLUSIONS

A cation-selective bipolar electrode array was successfully fabricated for the simultaneous determination of multiple cations using Prussian Blue thin films for optical readout. The work combines principles of potentiometric and optical sensors and may form the basis for new avenues in ion sensing. The approach described here makes it possible to realize optical sensors that respond in analogy to potentiometric sensing probes, with the same assumptions and the possibility for cross-correlation and traceability. The optical readout is achieved away from the sample and does not suffer from optical interference. Consequently, colored fruit juices were chosen as examples and were adequately assessed. The technology also offers advantages over established potentiometric sensors. Any number of PB-ISE bipolar electrodes can be inserted in parallel without increasing instrumental complexity. The readout is optical and can be achieved with a convenient imaging device. Potentiometric sensing arrays require complex individual wiring or light addressability to achieve this. Last, this work forms the foundation to achieve self-powered sensing devices where the optical signal is directly generated from the potential change at the ion-selective electrode, without the need for additional electronics or power sources, conceptually related to a recent example demonstrated by Rho et al.[52] This is currently in progress in our laboratory.

ASSOCIATED CONTENT

Supporting Information

The Supporting Information is available free of charge at https://pubs.acs.org/doi/10.1021/acs.analchem.0c01421.

Equilibrium theory, fabrication details and photographs of the setup, electrochemical and colorimetric behavior of Prussian Blue films, calibration curves for ion-selective electrodes, potential change during galvanostatic perturbation of ion-selective membranes, electrochemical and colorimetric reproducibility of bipolar electrode, and selectivity behavior (PDF)

AUTHOR INFORMATION

Corresponding Author

Eric Bakker − *Department of Inorganic and Analytical Chemistry, University of Geneva, Geneva 1211, Switzerland;* orcid.org/0000-0001-8970-4343; Email: eric.bakker@unige.ch

https://dx.doi.org/10.1021/acs.analchem.0c01421
Anal. Chem. 2020, 92, 9138−9145

Authors

Sutida Jansod − *Department of Inorganic and Analytical Chemistry, University of Geneva, Geneva 1211, Switzerland*

Thomas Cherubini − *Department of Inorganic and Analytical Chemistry, University of Geneva, Geneva 1211, Switzerland*

Yoshiki Soda − *Department of Inorganic and Analytical Chemistry, University of Geneva, Geneva 1211, Switzerland*

Complete contact information is available at: https://pubs.acs.org/10.1021/acs.analchem.0c01421

Notes

The authors declare no competing financial interest.

■ ACKNOWLEDGMENTS

We thank the Swiss National Science Foundation (SNSF) for financial support. S.J. especially thanks the Swiss Government Excellence Fellowship in support for her doctoral studies.

■ REFERENCES

(1) Zheng, G.; Patolsky, F.; Cui, Y.; Wang, W. U.; Lieber, C. M. *Nat. Biotechnol.* **2005**, *23* (10), 1294−1301.

(2) Gao, W.; Emaminejad, S.; Nyein, H. Y. Y.; Challa, S.; Chen, K.; Peck, A.; Fahad, H. M.; Ota, H.; Shiraki, H.; Kiriya, D.; Lien, D.-H.; Brooks, G. A.; Davis, R. W.; Javey, A. *Nature* **2016**, *529* (7587), 509−514.

(3) Albert, K. J.; Lewis, N. S.; Schauer, C. L.; Sotzing, G. A.; Stitzel, S. E.; Vaid, T. P.; Walt, D. R. *Chem. Rev.* **2000**, *100* (7), 2595−2626.

(4) Martinez-Olmos, A.; Capel-Cuevas, S.; López-Ruiz, N.; Palma, A. J.; de Orbe, I.; Capitán-Vallvey, L. F. *Sens. Actuators, B* **2011**, *156* (2), 840−848.

(5) Lapresta-Fernández, A.; Capitán-Vallvey, L. F. *Anal. Chim. Acta* **2011**, *706* (2), 328−337.

(6) Lapresta-Fernández, A.; Huertas, R.; Melgosa, M.; Capitán-Vallvey, L. F. *Anal. Chim. Acta* **2009**, *636* (2), 210−217.

(7) Bakker, E.; Pretsch, E. *Angew. Chem., Int. Ed.* **2007**, *46* (30), 5660−5668.

(8) Zdrachek, E.; Bakker, E. *Anal. Chem.* **2019**, *91* (1), 2−26.

(9) Alexander, P. W.; Dimitrakopoulos, T.; Hibbert, D. B. *Electroanalysis* **1998**, *10* (10), 707−712.

(10) Mourzina, Y. G.; Schubert, J.; Zander, W.; Legin, A.; Vlasov, Y. G.; Lüth, H.; Schöning, M. J. *Electrochim. Acta* **2001**, *47* (1), 251−258.

(11) Rudnitskaya, A.; Ehlert, A.; Legin, A.; Vlasov, Y.; Büttgenbach, S. *Talanta* **2001**, *55* (2), 425−431.

(12) Bratov, A.; Abramova, N.; Ipatov, A. *Anal. Chim. Acta* **2010**, *678* (2), 149−159.

(13) Dimitrakopoulos, T.; Alexander, P. W.; Hibbert, D. B. *Electroanalysis* **1996**, *8* (5), 438−442.

(14) Mueller, A. V.; Hemond, H. F. *Talanta* **2013**, *117*, 112−118.

(15) Pankratova, N.; Crespo, G. A.; Afshar, M. G.; Crespi, M. C.; Jeanneret, S.; Cherubini, T.; Tercier-Waeber, M.-L.; Pomati, F.; Bakker, E. *Environ. Sci.: Process. Impacts* **2015**, *17* (5), 906−914.

(16) Le Goff, T.; Braven, J.; Ebdon, L.; Chilcott, N. P.; Scholefield, D.; Wood, J. W. *Analyst* **2002**, *127* (4), 507−511.

(17) Martínez-Barrachina, S. l.; del Valle, M.; Matia, L.; Prats, R.; Alonso, J. *Anal. Chim. Acta* **2001**, *438* (1), 305−313.

(18) Di Benedetto, L. T.; Dimitrakopoulos, T. *Electroanalysis* **1997**, *9* (2), 179−182.

(19) Gutiérrez, M.; Alegret, S.; del Valle, M. *Biosens. Bioelectron.* **2007**, *22* (9), 2171−2178.

(20) Gallardo, J.; Alegret, S.; Muñoz, R.; De-Román, M.; Leija, L.; Hernández, P. R.; del Valle, M. *Anal. Bioanal. Chem.* **2003**, *377* (2), 248−256.

(21) Askim, J. R.; Mahmoudi, M.; Suslick, K. S. *Chem. Soc. Rev.* **2013**, *42* (22), 8649−8682.

(22) Rakow, N. A.; Suslick, K. S. *Nature* **2000**, *406* (6797), 710−713.

(23) Johnson, S. R.; Sutter, J. M.; Engelhardt, H. L.; Jurs, P. C.; White, J.; Kauer, J. S.; Dickinson, T. A.; Walt, D. R. *Anal. Chem.* **1997**, *69* (22), 4641−4648.

(24) Anzenbacher, J. P.; Lubal, P.; Buček, P.; Palacios, M. A.; Kozelkova, M. E. *Chem. Soc. Rev.* **2010**, *39* (10), 3954−3979.

(25) Wu, M.-S.; Liu, Z.; Shi, H.-W.; Chen, H.-Y.; Xu, J.-J. *Anal. Chem.* **2015**, *87* (1), 530−537.

(26) Liu, C.; Wang, D.; Zhang, C. *Sens. Actuators, B* **2018**, *270*, 341−352.

(27) Xu, W.; Fu, K.; Ma, C.; Bohn, P. W. *Analyst* **2016**, *141* (21), 6018−6024.

(28) Crespo, G. A.; Mistlberger, G.; Bakker, E. *J. Am. Chem. Soc.* **2012**, *134* (1), 205−207.

(29) Zhai, J.; Yang, L.; Du, X.; Xie, X. *Anal. Chem.* **2018**, *90* (21), 12791−12795.

(30) Jaworska, E.; Michalska, A.; Maksymiuk, K. *Electrochim. Acta* **2018**, *284*, 321−327.

(31) Jansod, S.; Cuartero, M.; Cherubini, T.; Bakker, E. *Anal. Chem.* **2018**, *90* (11), 6376−6379.

(32) Jansod, S.; Bakker, E. *ACS Sens.* **2019**, *4*, 1008−1016.

(33) Niklasson, G. A.; Granqvist, C. G. *J. Mater. Chem.* **2007**, *17* (2), 127−156.

(34) Hoshino, K.; Okuma, M.; Terashima, K. *J. Phys. Chem. C* **2018**, *122* (39), 22577−22587.

(35) Hoshino, K.; Nakajima, R.; Okuma, M. *Appl. Surf. Sci.* **2014**, *313*, 569−576.

(36) Cutler, C. A.; Bouguettaya, M.; Reynolds, J. R. *Adv. Mater.* **2002**, *14* (9), 684−688.

(37) Nossol, E.; Zarbin, A. J. G. *Sol. Energy Mater. Sol. Cells* **2013**, *109*, 40−46.

(38) Liu, X.; Zhou, A.; Dou, Y.; Pan, T.; Shao, M.; Han, J.; Wei, M. *Nanoscale* **2015**, *7* (40), 17088−17095.

(39) Liana, D. D.; Raguse, B.; Gooding, J. J.; Chow, E. *ACS Appl. Mater. Interfaces* **2015**, *7* (34), 19201−19209.

(40) Chow, E.; Liana, D. D.; Raguse, B.; Gooding, J. J. *Aust. J. Chem.* **2017**, *70* (9), 979−984.

(41) Itaya, K.; Shibayama, K.; Akahoshi, H.; Toshima, S. *J. Appl. Phys.* **1982**, *53* (1), 804−805.

(42) Robin, M. B. *Inorg. Chem.* **1962**, *1* (2), 337−342.

(43) Neff, V. D. *J. Electrochem. Soc.* **1978**, *125* (6), 886.

(44) Kim, L. T. T.; Gabrielli, C.; Perrot, H.; Garcia-Jareno, J.; Vicente, F. *Electrochim. Acta* **2012**, *84*, 35−48.

(45) Ho, K.-C.; Lin, C.-L. *Sens. Actuators, B* **2001**, *76* (1), 512−518.

(46) Nguyen, B. T. T.; Ang, J. Q.; Toh, C.-S. *Electrochem. Commun.* **2009**, *11* (10), 1861−1864.

(47) Ghosh, T.; Chung, H.-J.; Rieger, J. *Sensors* **2017**, *17* (11), 2536.

(48) Krishnan, V.; Xidis, A. L.; Neff, V. D. *Anal. Chim. Acta* **1990**, *239*, 7−12.

(49) Itaya, K.; Uchida, I.; Neff, V. D. *Acc. Chem. Res.* **1986**, *19* (6), 162−168.

(50) Soda, Y.; Bakker, E. *ACS Sens.* **2019**, *4* (12), 3093−3101.

(51) Erenas, M. M.; de Orbe-Payá, I.; Capitan-Vallvey, L. F. *Anal. Chem.* **2016**, *88* (10), 5331−5337.

(52) Rho, J.; Yeon, S. Y.; Chung, T. D. *Anal. Chem.* **2020**, 1 DOI: 10.1021/acs.analchem.0c00142.